Beam Physics Note
TRI-BN-19-02
April 8, 2019

TRANSOPTR Implementation of the MEBT Beamline

Olivier Shelbaya

TRIUMF

Abstract: Under the TRIUMF High-Level Applications (HLA) framework, the linear envelope optics code TRANSOPTR has been extended to include the ISAC Medium Energy Beam Transport (MEBT) section. This note presents the implementation and a benchmark comparison of the TRANSOPTR-MEBT simulation with trace3D, used up to this point to perform the envelope optics computations used to produce MEBT tunes.

Contents

1 Introduction

TRANSOPTR, the linear optics code which computes the evolution of the second moments of the beam distribution through various ion-optic transport elements [1] [2], including in presence of space charge [3] has been extended to include the ISAC Medium Energy Beam Transport (MEBT) section. This section transports beams accelerated through the ISAC radiofrequency quadrupole (RFQ) at an energy of 153keV/u into the ISAC Drift Tube Linac (DTL), enabling further acceleration to a maximum of 1.5MeV/u for high-energy delivery to ISAC's experimental stations [4].

The MEBT line, shown in Figure 1, possesses no experimental destinations. In this respect, it is very much an integral part of the ISAC-I linear accelerator, allowing for a longitudinal and transverse matching between the RFQ and the ISAC Drift Tube Linac (DTL), a 7 tank interdigital H-mode (IH) linac based upon the KONUS beam dynamic design [5]. While the transverse match is accomplished using a sequence of 13 magnetic quadrupoles and two 45° bending magnets, the longitudinal match is accopmlished using two separate RF bunching cavities.

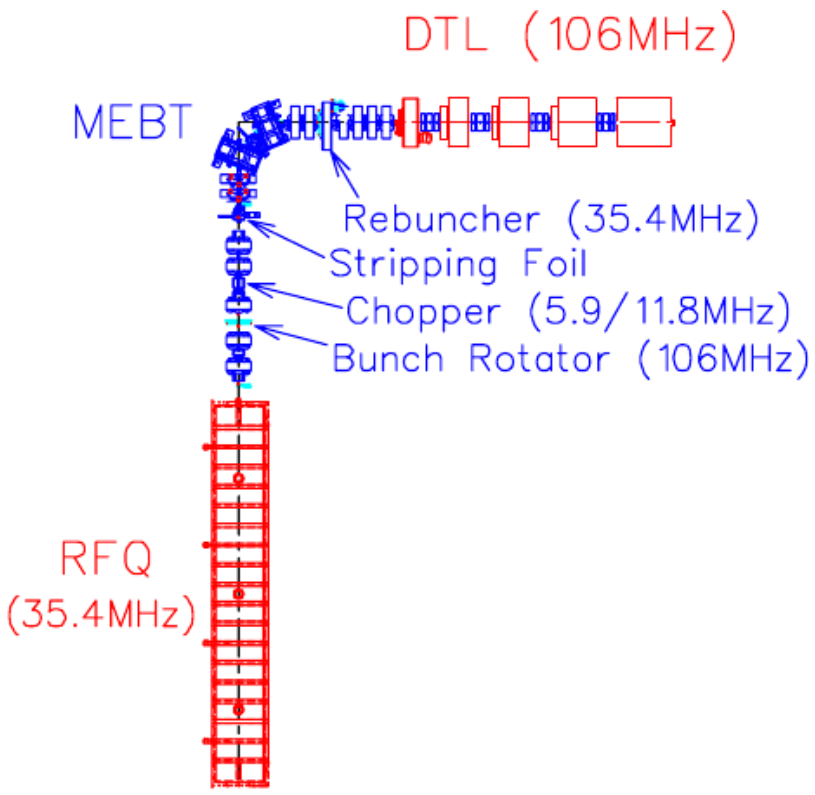

Figure 1: Overview of the ISAC-I MEBT section, joining RFQ and DTL, with labeled RF devices.

An RF chopper operating at 5 or 11MHz removes so-called RFQ satellite peaks, which consist of partially filled RFQ output shots which represent two out of every three accelerating buckets in the linac. This is a consequence of the separated pre-bunching scheme

of the ISAC RFQ, which uses a three-harmonic psuedosawtooth modulation with a master frequency of 11MHz, to accopmlish a time focus at the RFQ's acceptance [6].

A stripping foil in the section, before the horizontal bending magnets, allows for an increase in charge state, enabling two separate functions:

1. Charge-selection filtration of unwanted beam contaminants transmitting the RFQ, and
2. Matching between the higher RFQ acceptance (A/q $\leq$ 30) and the DTL (2 $\leq$ A/q $\leq$ 7).

This note presents the implementation of the above in `TRANSOPTR`, in addition to a comparison with `trace3D` and a discussion of the details of the implementation. It is further noted that this note does not intend to make a commentary or an evaluation of the performance of either `TRANSOPTR` or `Trace-3D`. Rather, the present work is intended to demonstrate that the novel MEBT beamline implementation in `TRANSOPTR` produces a beam envelope which agrees with `Trace-3D` predictions and will therefore be suitable for use in the computation and analysis of ISAC high-energy tunes.

2 High-Level Application Implementation

Under the TRIUMF High-Level Applications (HLA) framework [7], the traditional `TRANSOPTR` element sequence stack `sy.f` is automatically generated through a python wrapper routine, which reads in the requisite sequence of elements from a central database. This database, known as the `/acc` database, formatted in `xml`, contains a sequential ordering of all transport, diagnostic and accelerating elements present along a given beamline segment.

Within the database, groups of elements are broken down into sequences, which consist of the smallest possible number of sequential elements which define a unique path. Since, as previously stated, the only possible path in MEBT starts at the RFQ output and ends at DTL injection, it is natural that the MEBT section be defined as a sequence, labeled `mebt_db0`, referring to the starting diagnostic box immediately following the ISAC RFQ.

While the sequence `xml` file contains the locations of all elements present in the beamline, including steering elements, beam diagnostics and aperture constrictions, for the purposes of the present note, these will be implicitely omitted, in favor of beamline optical elements such as quadrupoles and RF cavities. The rationale for doing so is that both diagnostics and steerers are not used in `TRANSOPTR`, which assumes an on-axis beam at all times and locations along the beampath. This is not to say that diagnostic locations are unimportant. On the contrary, knowing their precise location is crucial to predict measured beam envelope behavior. However, given that they do not affect the envelope `TRANSOPTR`, in the present note their presence is implicitely acknowledged but not explicitely discussed. Consequently, the focus will be placed on ion-optical elements such as quadrupoles, bending magnets and RF cavities.

3 Sequence `mebt_db0` and Source Material

MEBT Quadrupoles follow a design specification providing an 18.0 cm effective length [8], designed to allow transport of beams with $1 \leq$ A/q ≤ 30 from the RFQ. MEBT sequence element positioning and lengths were verified using TRIUMF design drawings listed in Table 1. Each drawing was obtained from the TRIUMF Design Office, representing the as-installed MEBT beamline. The reference units used in each drawing are inches, and a conversion factor of 25.4 mm per inch was used for final construction of the `/acc` database.

sequence `mebt_db0`			
Start `IBP0436D.dwg` (x,y)		End `IBP0436D.dwg` (x,y)	
(217.679",76.798")		(32.614",76.798")	
Design Drawing		Figure 2	
Element Name	Element Type	Position S[mm]	Length L[mm]
start sequence	`marker`	0.000	0.000
MEBT:Q1	`MQuad`	809.625	180.000
MEBT:Q2	`MQuad`	1414.450	180.000
ISAC1:ROTR	`linac`	1746.415	122.500
MEBT:Q3	`MQuad`	2071.675	180.000
MEBT:Q4	`MQuad`	2892.425	180.000
MEBT:Q5	`MQuad`	3324.225	180.000
MEBT:STRP5	`marker`	4049.500	0.000
MEBT-ROTATE	`rt` (-45°)	4049.500	0.000
Start `IBP0480D.dwg` (x,y)		End `IBP0480D.dwg` (x,y)	
(144.938",71.487")		(84.405",176.302")	
Design Drawing		Figure 3	
MEBT:Q6	`MQuad`	4440.575	180.000
MEBT:Q7	`MQuad`	4700.615	180.000
MEBT:MB1	`mb`	5268.460	235.600
MEBT:MB2	`mb`	6104.080	235.600
MEBT:Q8	`MQuad`	6671.894	180.000
MEBT:Q9	`MQuad`	6971.944	180.000
Start `IBP0500D.dwg` (x,y)		End `IBP0500D.dwg` (x,y)	
(186.131",71.107")		(51.920",71.107")	
Design Drawing		Figure 4	
ISAC1:MEBT	`linac`	7319.729	199.263
MEBT:Q10	`MQuad`	7687.656	180.000
MEBT:Q11	`MQuad`	7985.346	180.000
MEBT:Q12	`MQuad`	8283.034	180.000
MEBT:Q13	`MQuad`	8580.723	180.000
end sequence	`marker`	8904.435	0.000

Table 1: Sequence `mebt_db0`, showing source design drawings (`.dwg` files) with reference start and end coordinates from which elements and their centerpoint positions along the optical axis, S in millimeters were extracted. Note: all MEBT design drawings use inches as reference units, however the `/acc` database by convention is defined in metric units. The `TRANSOPTR` element (subroutine) type, in addition to the element length are also displayed. All element positions are referenced to the drawing listed above their respective location in the table.

The drift distances at all locations are computed as representing the path length through the optical axis defining the beam path. Given that the `/acc` database defines drift distances with zero-insertion length for optical elements, this means that drifts are always computed as the integrated arclength between the optical centers of adjacent elements. For the example of two sequential magnetic quadrupoles, this is a line segment from one quadrupole's centerpoint to the next. However, for the case of the 45° bending magnets, this corresponds to the length of the circular path defining the design trajectory through the magnet.

Table 1 shows the entire span of `mebt_db0` as implemented in the `/acc` database, showing the three distinct sub-sequence segments, each referenced to the drawings specified in the table. The first segment, which spans MEBT:Q1 to Q5, starts at the output of the RFQ, specifically the vacuum flange point defined by the coordinates (217.679",76.798") on drawing `IBP0436D.dwg` and ends at the location of the stripping foil, shown in Figure 2, as indicated in Table 1.

A `TRANSOPTR` rotate call, which rotates the transverse phase space by -45° is also placed at the location of the MEBT stripping foil. By design, magnetic quadrupoles between the RFQ and the foil (MEBT:Q1 to Q5) are installed at a 45° tilt in the x-y plane, matching the orientation of local (x,y) axes defined by the RFQ vanes, themselves rotated by 45°. As the quadrupoles are engineered to sit on the beamline at a 0° angle, the remaining 8 quadrupoles (MEBT:Q8 to Q13) were installed following their design, which effectively introduces a 45° transverse rotation with regards to the first 5 quadrupoles in MEBT. As will be shown later, the design MEBT tune includes a double (x,y) focus on the foil, which produces a round beamspot, after which the remainder of the x-y plane in MEBT follows the standard orientation, with x being horizontal to the ground and y-vertical.

Next, the stripping foil location is used as a starting reference for elements MEBT:Q6 to Q9, which includes the MEBT bending magnets, shown in Figure 3. Presently in the `TRANSOPTR` implementation of the MEBT line, there is no stripping foil option available in a self-contained subroutine. However, based on known stripping foil dynamics and behavior [9], work is underway to implement a charge selection routine, which will allow the simulation of stripping foil use, complete with the corresponding emittance growth which is expected.

At the rough midpoint of the MEBT sequence lie both 45° magnetic dipoles which define the bend from RFQ to DTL. Both magnets, possessing a design radius of curvature of 300cm, which results a curved optical path length of 235.6mm. The positions defining MEBT:MB1 and MB2 in Table 1 correspond to the midpoint along this curved reference trajectory. In other words, the path length from MEBT:Q7 to MEBT:MB1 (see Figure 3) is defined as the straight segment from Q7 to the beginning of the curved trajectory through the magnet, plus half of the magnet path length.

Finally, the sequence `mebt_db0` ends with the linear segment defined by the quadrupoles MEBT:Q8 to Q13, leading into DTL Tank1, shown in Figure 4. This includes the MEBT Rebuncher, which is used to establish a longitudinal focus at DTL Tank1. As specified in Table 1, the sequence ends 323.712mm beyond MEBT:Q13 midpoint, which corresponds to the outer surface of the first DTL tank.

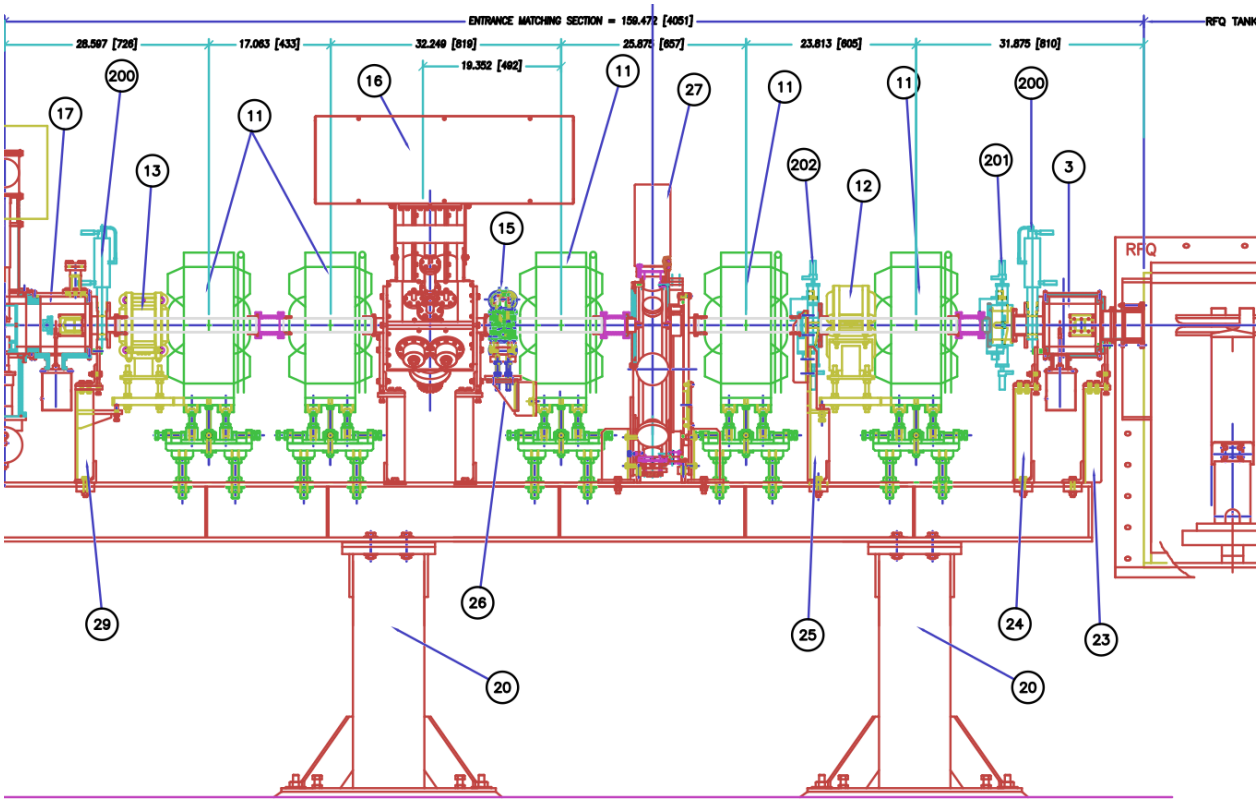

Figure 2: Design drawing `IBP0436D.dwg`, showing the elements represented in the `/acc` database definition for sequence `mebt_db0`, namely MEBT:Q1 to MEBT:Q5, visible in green, with Q1 on the right side and Q5 on the left. Note the improprely represented radial matching section on the RFQ-vanes, shown on the high-energy end of the RFQ. The beam propagation direction runs from right to left.

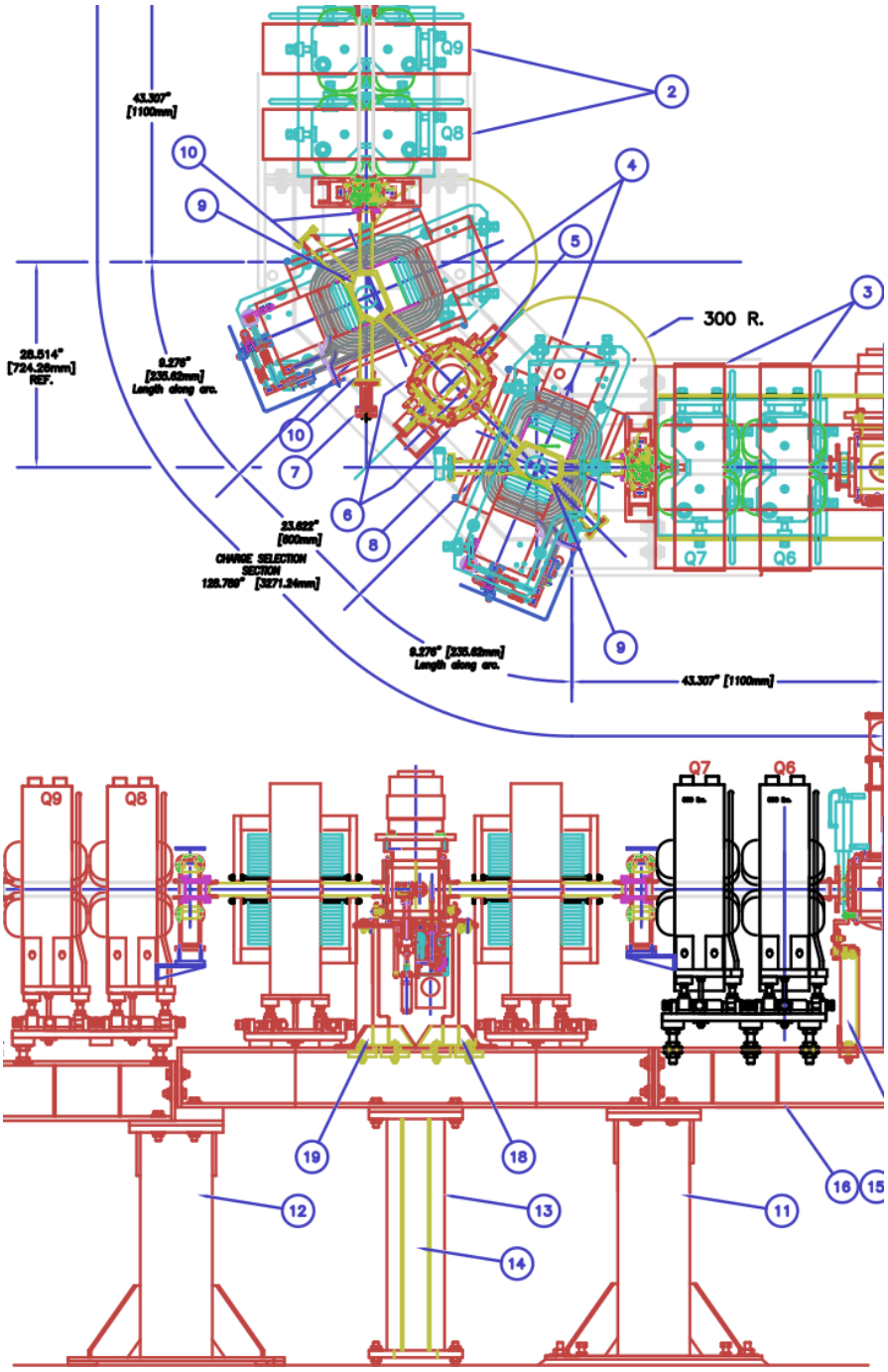

Figure 3: Design drawing `IBP0480D.dwg`, showing the elements represented in the `/acc` database definition for sequence `mebt_db0`, namely MEBT:Q6 to MEBT:Q9, including MEBT:MB1 and MEBT:MB2. The beam propagation direction runs from right to left on the bottom figure.

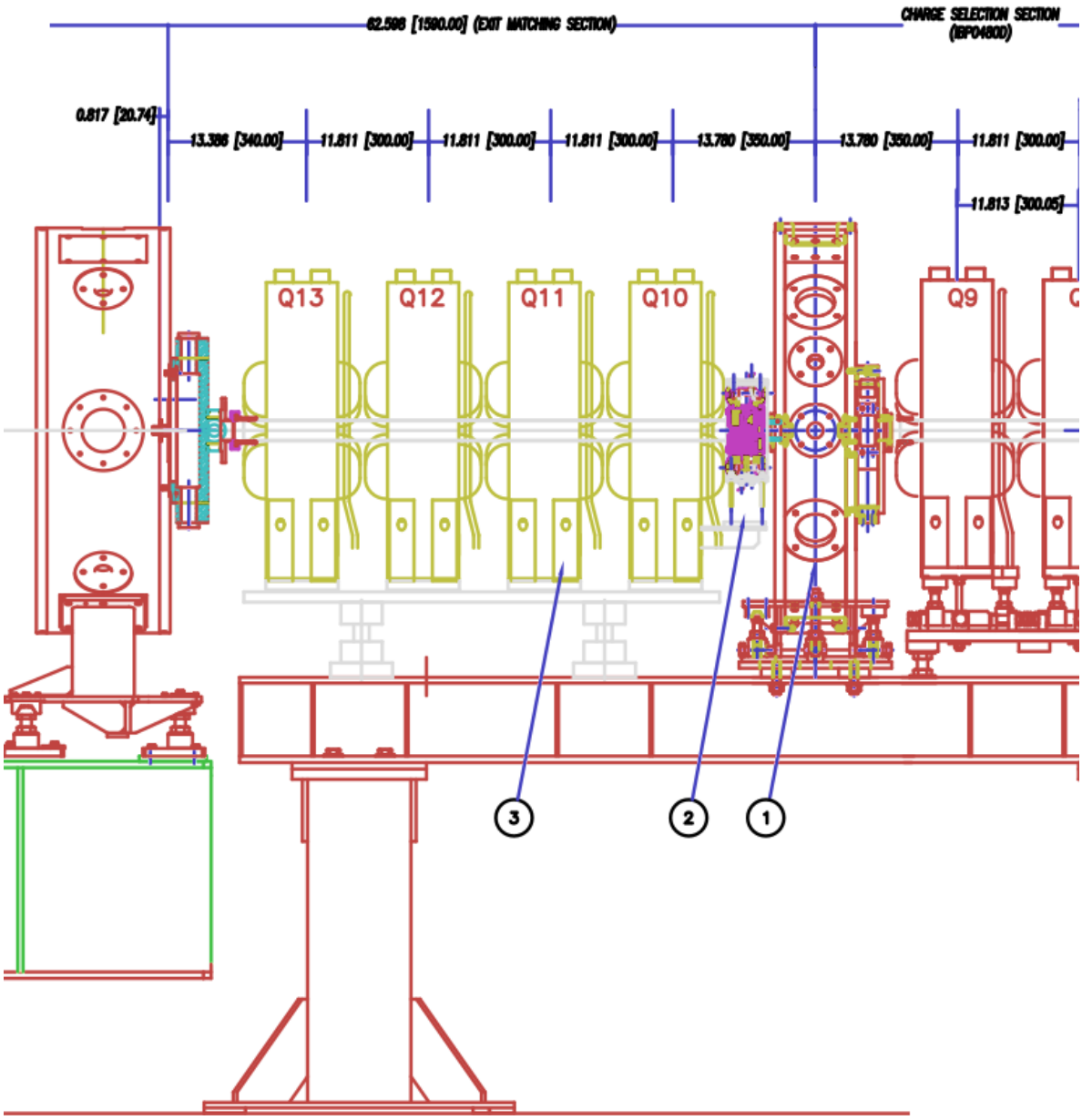

Figure 4: Design drawing `IBP0500D.dwg`, showing the elements represented in the `/acc` database definition for sequence `mebt_db0`, namely MEBT:Q10 to MEBT:Q13. The sequence `mebt_db0` ends at the outer surface of DTL Tank1. The beam propagation direction runs from right to left. Note that the `Trace-3D` subsequence representing this segment omits the MEBT Rebuncher, instead starting at its output.

3.1 MEBT RF Cavities

`TRANSOPTR` accelerating (or bunching) simulations rely upon calls to the subroutine `linac`, which itself expects as input a handfull of cavity design parameters. These include the RF phase setting of the cavity and the operating frequency in MHz. As is outlined in Reference [10], for the case of axially symmetric RF accelerating geometries, the F-matrix representing the cavity effects upon the moments of the beam distribution may be expressed as:

$$\mathbf{F_R}(s) = \begin{pmatrix} 0 & \frac{1}{P_0} & 0 & 0 & 0 & 0 \\ \mathcal{A}(s) & 0 & 0 & 0 & 0 & 0 \\ 0 & 0 & 0 & \frac{1}{P_0} & 0 & 0 \\ 0 & 0 & \mathcal{A}(s) & 0 & 0 & 0 \\ 0 & 0 & 0 & 0 & \frac{\beta'}{\beta} & \frac{1}{\gamma^2 P_0} \\ 0 & 0 & 0 & 0 & \mathcal{B}(s) & -\frac{\beta'}{\beta} \end{pmatrix} \tag{1}$$

with the functions:

$$\mathcal{A}(s) = -\frac{q}{2\beta c}\left(\mathcal{E}'(s)C - \mathcal{E}(s)S\frac{\omega\beta}{c}\right) \tag{2}$$

$$\mathcal{B}(s) = \frac{q\mathcal{E}(s)\omega S}{\beta^2 c^2} \tag{3}$$

where the parameters $S = \sin(\omega t_0 + \theta)$ and $C = \cos(\omega t_0 + \theta)$ and $\mathcal{E}(s)$ & $\mathcal{E}'(s)$ is the on-axis electric field and its derivative with respect to s, the distance along the optical axis. Providing this field mapping is therefore indispensible for implementing the envelope simulation.

3.2 Attempted Bead Pull Electric Field Extraction

3.2.1 Preface

The present subsection details an attempt made to extract the on-axis electric field maps from existing literature. Seeing as the `TRANSOPTR` implementation of the MEBT section is a novel project, no suitable field maps were readily available in a format suitable for the subroutine `linac`. On-axis electric fields may be obtained from bead pulling measurements, available in various conference proceedings, namely [11], [12], [13], [14] and [15]. An attempt was therefore made to extract the electric fields from the referenced bead pulling data.

The available bead-pull measurements in the above references present two main challenges. First, the electric field which is extracted is an absolute magnitude and is positive along its entire domain. Second, due to the finite size of the bead and other experimental factors, the data may suffer from noise. Bead pulls for the Bunch Rotator (in addition to

DTL Bunchers 1,2 and 3) are shown in Figure 5.

3.2.2 Attempted Extraction

Bead-pull field map extraction attempted to alleviate the two aformentioned challenges. Regarding the issue of electric field sign loss, inspection of Figure 5 reveals that, in order to restore the proper electric field morphology along the s-axis, it would be necessary to invert two of the three peaks, to provide `TRANSOPTR` with a proper electric field map, which represented the field profile at a discrete point in time, with alternatingly positive and negative peaks between adjacent gaps. Note that the fields in the figure do not ever reach zero, but rather attain a noise level, a byproduct of the finite bead size integrating the field at its location. Interpreting this data therefore necessitates applying some form of data processing, to avoid introducing discontinuities.

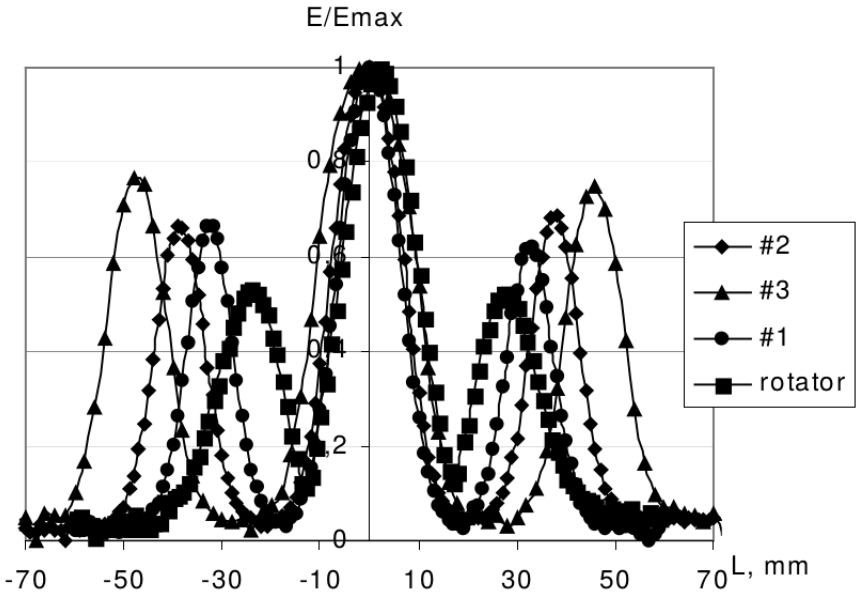

Figure 5: Bead pull measurement extracted normalized on-axis electric field, obtained from [15], showing the on-axis electric field for the Bunch Rotator and DTL Bunchers 1,2 and 3.

A further complication lies in the obtention of the original source data from the bead pulls. Several attempts were made by the author to obtain this information in its original format. Following several lines of investigation however, it was concluded by the author of the present note that obtaining this data is not possible. This may be attributed to two facts:

- The measurements were carried nearly 20 years ago, and
- The source data was not saved on controlled information systems

Thus, due to both the age of these measurements, staff rollover, changes in computing technology including staff members periodically changing personal computers, the above data is at present considered lost. Nevertheless, an attempt was made to extract this data from the available figures, using the image digitization software `engauge`, which allows for the extraction of datasets from various image formats, including `pdf` [16]. Systematic errors from the digitization extraction process are estimated as spanning a few pixels in both x and y dimensions, producing a variable error which ultimately depends on the range of the dataset x and y axes. To provide a reasonable example for these values, the author estimates an uncertainty corresponding to the linewidth on the source image, producing a systematic error whose value is on the order of 1%. Digitization of one of the curves shown in Figure 5, including the inversion of the odd-numbered peaks is shown in Figure 6. As an initial test, the field sign was inverted at the location of the starts/ends of the tubes in the accelerating structure.

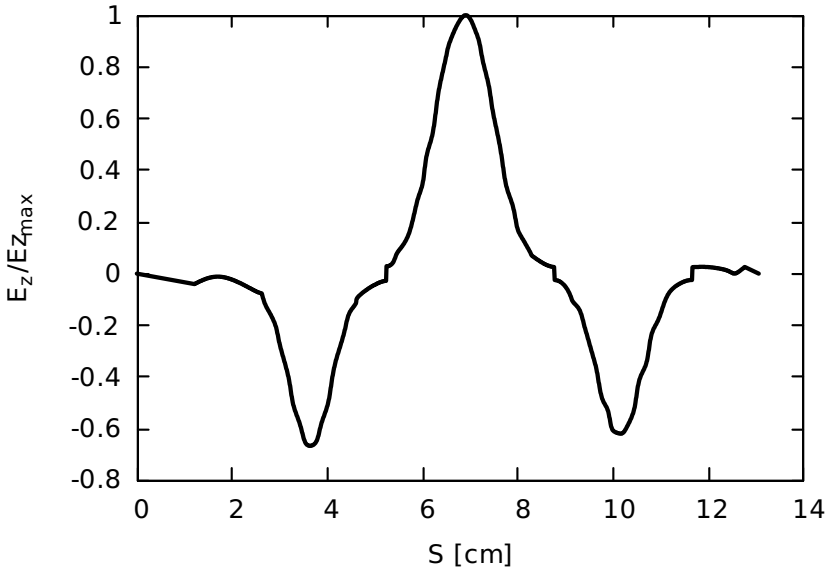

Figure 6: Digitized, extracted and restored normalized on-axis electric field, obtained from Figure 5, showing noise from the measurement in addition to sharp discontinuities introduced from inverting the dataset.

Note that data extraction necessitated full line extraction, including the artifical trendlines, which are meant to guide the eye but do not represent an actual electric field profile. It was found that attempting to extract individual datapoints was too difficult due to graph datapoint clutter in the regions where the data overlaps, due to the monochrome plotting which was used. Despite this, usage of extracted bead pulls still presents a series of issues with regards to the interpretation of the data. The issue of noise is the most pressing. Also, as previously discussed, since the bead pull offers an absolute value, when attempting to restore the original field profile, inverting peaks introduces sharp discontinuities (therefore sharp electric field derivatives), which will result in unphysical kicks to the beam distribution as it traverses the restored field map.
Following numerous attempts, the idea of field map digitization and postprocessing was abandoned, due to the excessive number of approximations and choices which had to be

Cavity	ref. DWG
Bunch Rotator	IRF0965D.dwg*
Re-buncher	IRF1811D.dwg

Table 2: Design drawings obtained from TRIUMF Design Office for each of the two bunching MEBT RF cavities. * Note, for the Bunch Rotator, the drawing is a digitized adaptation from the original INR-RAS schematic. The digitization process failed to properly interpret the original cyrillic characters from the Russian drawing rendering much of it unreadable. Further, possibly as a byproduct of digitization, the dimensions shown in the drawing disagree with the digitized coordinate by a ratio of 2:1. Further, the drawing's TRIUMF standard footnote erroneously claims that the dimensions are inches. In fact, the dimensions of the Russian drawing are millimeters. In practice, this means that attempting to measure distances in any digital drawing software will produce units that must be multiplied by 2 and are actually mm, not inches.

made, each considered to introduce supplemental systematic errors. Instead, an electrostatic simulation suite, Opera2D was used, combined with the original design drawings, to produce on-axis electrostatic field maps for use in the TRANSOPTR linac calls.

3.3 Opera2D RF Cavity Simulations

Using the electrostatic code Opera2D [17], in addition to the original digitized design drawing, shown in Table 2, a Bunch Rotator on-axis electric field profile suitable for TRANSOPTR F-matrix computation were produced, shown in Figure 9. The physical dimensions defining the tube gaps and other physical parameters used in the simulation are listed in Table 3. The tube geometry, as implemented in Opera2D features rounded edges, whose radius of curvature was extracted from the same design drawings, shown in Figure 7.

Parameter	Value [in]
Start	0.0000
ground tube end	0.9375
tube 1 start	1.2271
tube 1 end	2.1298
tube 2 start	2.6732
tube 2 end	3.5759
ground tube start	3.8189
ground tube end	4.8228
aperture radius	0.2756
radial tube thickness	0.3150
inner-tube rounding radius	0.07874
outer tube rounding radius	0.19686
full field-map length	4.8228

Table 3: Physical dimensions extracted from drawing IRF0965D.dwg for the Bunch Rotator.

The MEBT Rebuncher was also simulated in Opera2D, based on the design drawing specified in Table 4, shown in Figure 8, with simulation parameters specified in Table 4. The Rebuncher on-axis electric field is shown in Figure 10.

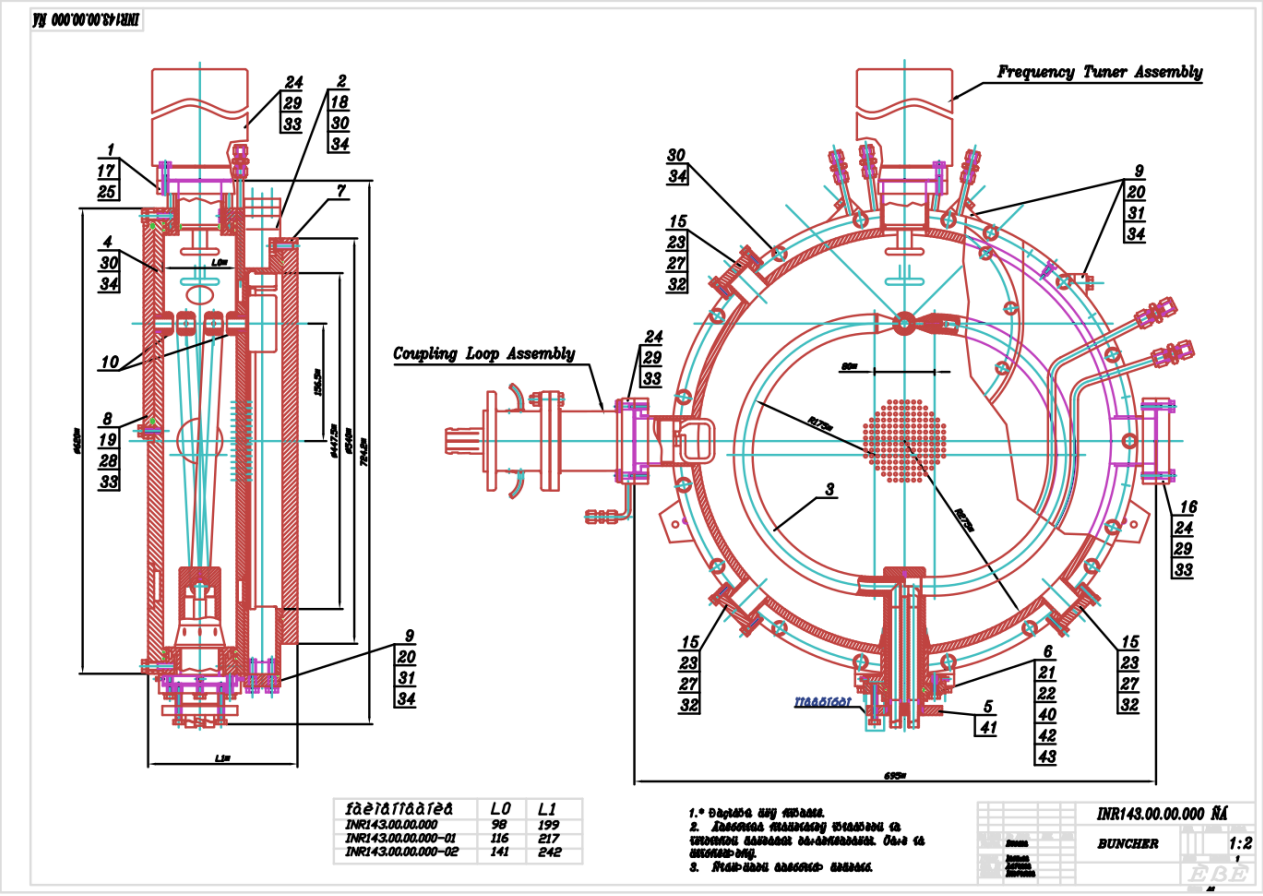

Figure 7: Digitized design drawing for the MEBT Bunch Rotator, originally from INR-RAS, used for `Opera2D` field map generation. Note the transliteration errors representing original cyrillic characters. Dimensions as shown in the drawing are in millimeters, and are valid. Obtained from the TRIUMF Design Office.

Parameter	Value [in]
Start	0.0000
ground tube end	1.6940
tube 1 start	3.1115
tube 1 end	4.7335
ground tube start	6.1510
ground tube end	7.8450
aperture radius	0.3937
radial tube thickness	0.2524
inner-tube rounding radius	0.1262
outer tube rounding radius	0.1262
full field-map length	7.8450

Table 4: Physical dimensions extracted from drawing `IRF1811D.dwg` for the MEBT Rebuncher.

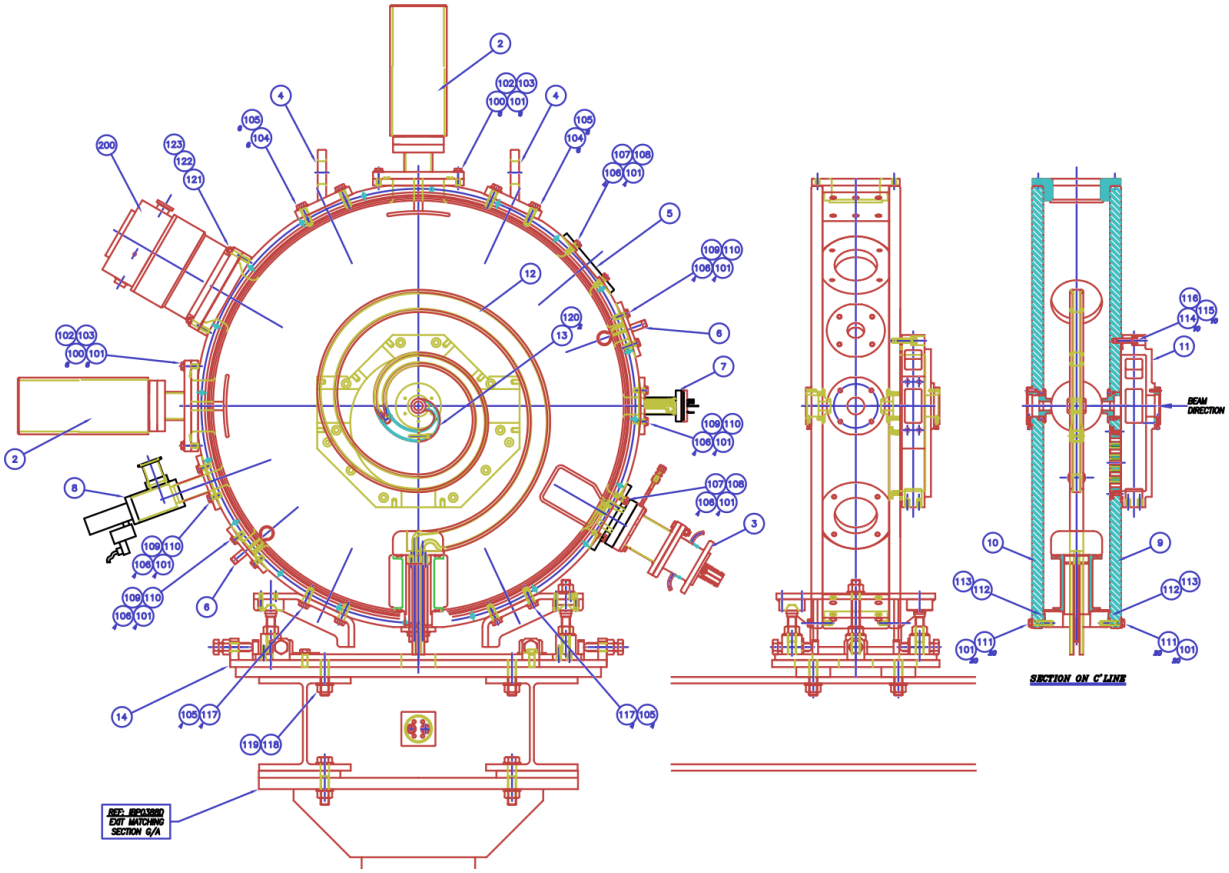

Figure 8: Digitized design drawing for the MEBT Rebuncher, used for `Opera2D` field map generation. Obtained from the TRIUMF Design Office.

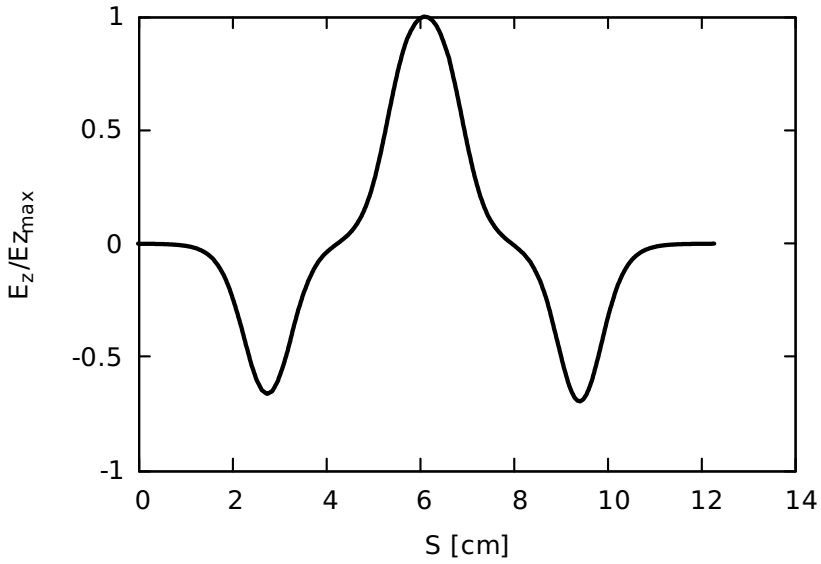

Figure 9: `Opera2D` simulated normalized on-axis electric field for the MEBT Bunch Rotator, using the parameters specified in Table 3.

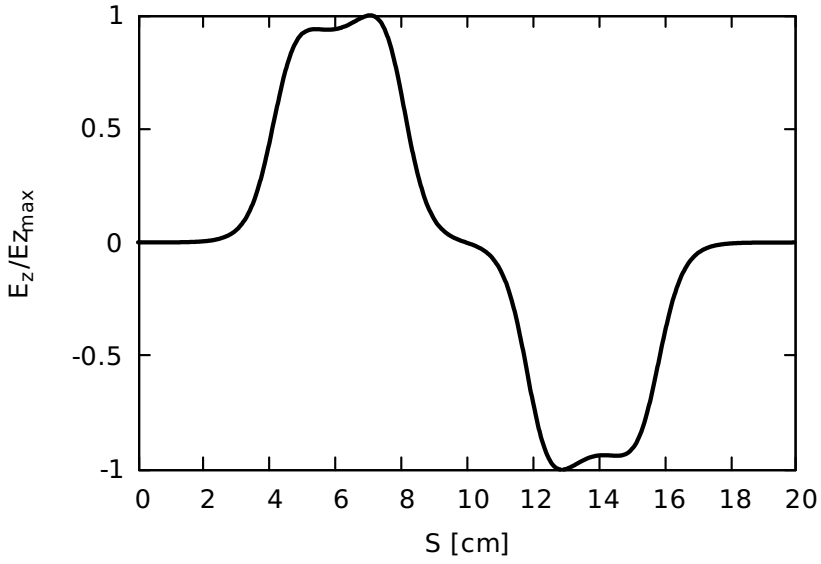

Figure 10: `Opera2D` simulated normalized on-axis electric field for the MEBT Rebuncher, using the parameters specified in Table 4.

4 Comparison with Trace3D

The envelope calculation code Trace3D has, up to this point, been the principal tune investigation and computation software used for the MEBT section. The code, developed at Los Alamos National Laboratory, computes the envelopes of bunched beams and includes computation of linear space charge forces [18]. As TRANSOPTR is intended to supplant and obviate Trace3D usage for ISAC high energy tune computation and investigation, a quantitative envelope comparison for identical beam input parameters is in order.

A mass 30, 4.5MeV (0.15MeV/u) beam, corresponding to the upper design mass-to-charge acceptance limit of the RFQ, was simulated through MEBT in both Trace-3D and TRANSOPTR. The parameters used for the simulation are shown in Table 5.

param.	value	unit
m	27 944.34	MeV/c^2
E	4.50	MeV
I	0.0	mA
Q_1	1	-
Q_6	5	-

Table 5: List of beam parameters used for the TRANSOPTR & Trace-3D comparison. Q_1 is the charge state before the foil, Q_6 is the charge state after the foil, starting at MEBT:Q6.

4.1 Trace-3D Simulation

The Trace-3D implementation for the MEBT beamline is segmented into three sections, following those outlines in Table 1. As it is presently used MEBT tune computation, the model excludes simulation of the MEBT stripping foil. Instead, the foil effects are accounted for by increasing the charge state and input transverse and longitudinal emittances between the segments containing MEBT:Q5 and MEBT:Q6.

The present simulation transported an RFQ output beam, mass 30, charge state 1, at an energy of 0.15MeV/u up to the stripping foil, where its charge state was increased to 5. Inspection of Figure 11, showing the sub-sequence containing MEBT:Q1 to Q5, shows that the MEBT tune is designed to produce a double transverse focus in (x, y) on the stripping foil. In the following segment, shown in Figure 12, showing the sub-sequence containing MEBT:Q6 to Q9, one can observe how the input beam distribution has simply seen its emittance roughly doubled, and the charge state has been increased from 1 to 5. The effect of the bunch rotator may also be seen in Figure 11, as seen on the longitudinal envelope. It is noted that in the formalism of Trace-3D, RF cavities are approximated as discrete kicks to the envelope, which produces a sharp kink on the longitudinal envelope in Figure 11.

The two 45° bending magnets MEBT:MB1 & MB2's effect on the beam envelope is visible in Figure 12, with the final focus through MEBT:Q9 producing a transverse match at the location of the MEBT Rebuncher. The effect of the rebuncher, omitted from the original Trace-3D simulation is implicit, visible at the start of Figure 13, in which the longitudinal envelope starts off with a much broader emittance. The longitudinal twiss parameters at the input are chosen to produce a time focus at the very end of the sub-sequence defined from MEBT:Q10 to Q13, coinciding with the input of the first DTL tank.

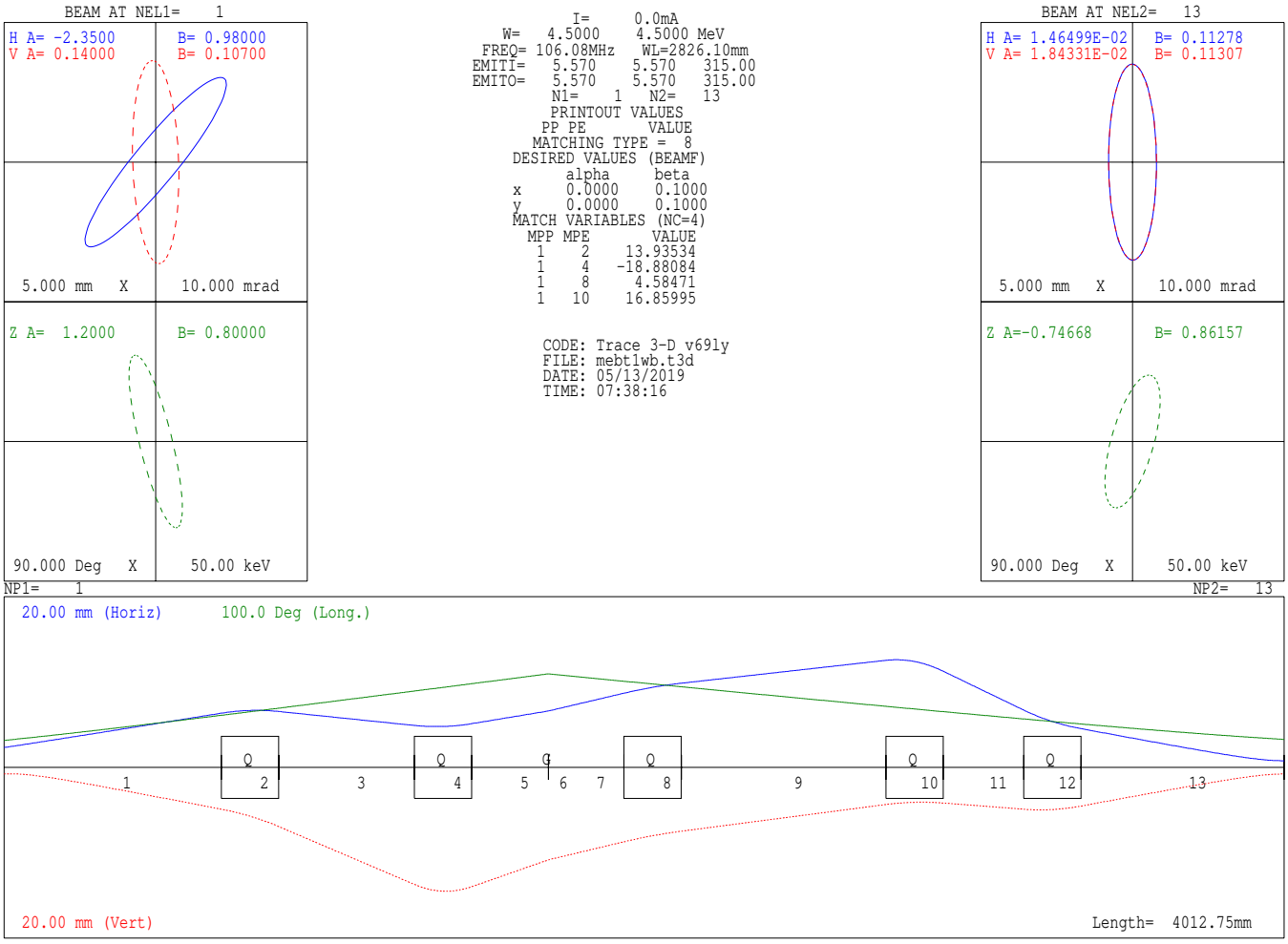

Figure 11: `Trace-3D` envelope simulation of sub-sequence spanning MEBT:Q1 to MEBT:Q5. The horizontal envelope and its parameters are shown in blue, horizontal in red and longitudinal in green. The input beam ellipses containing $4\epsilon_{RMS}$ are shown on the left hand side, with A and B representing the Twiss parameters α and β, while the output distributions are on the right hand side. The input and output beam emittances are visible in the top center, labeled EMITI and EMITO, respectively, and have units of mm*mrad for transverse and deg*keV for longitudinal. The beam envelopes are shown at the bottom, following the same color convention. The location and lengths of quadrupoles are represented by the squares labeled Q, while the approximated bunch rotator is visible as a short vertical line labeled G (RF Gap). Drifts are represented by a black horizontal line at the lower graph midplane. Finally, the numbers on the lower graph, spanning 1 to 13, sequentially label all elements called in the simulation. Quadrupole gradients are shown in Table 6.

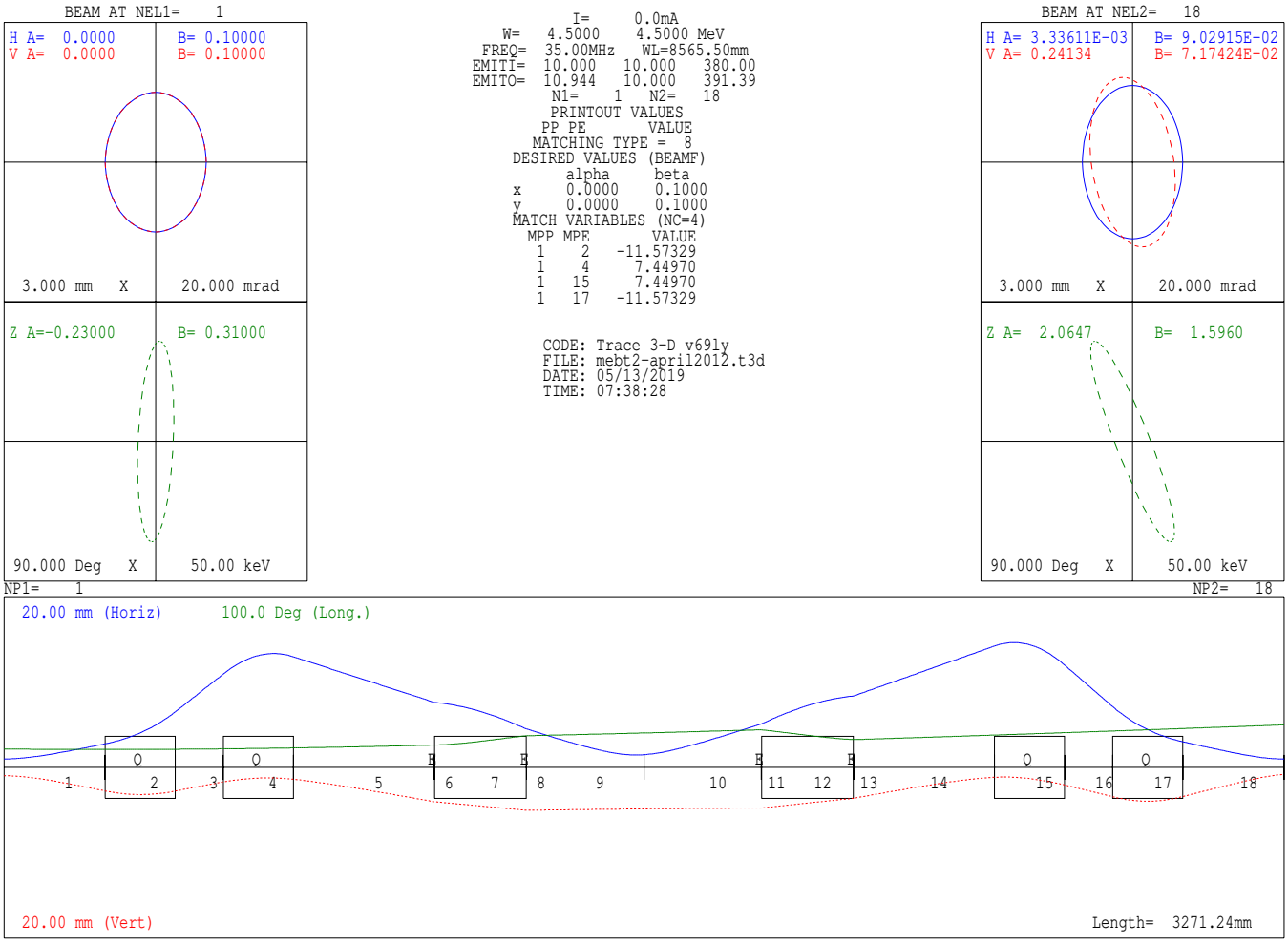

Figure 12: `Trace-3D` envelope simulation of sub-sequence spanning MEBT:Q6 to MEBT:Q9. The horizontal envelope and its parameters are shown in blue, horizontal in red and longitudinal in green. The input beam ellipses containing $4\epsilon_{RMS}$ are shown on the left hand side, with A and B representing the Twiss parameters α and β, while the output distributions are on the right hand side. The input and output beam emittances are visible in the top center, labeled EMITI and EMITO, respectively, and have units of mm*mrad for transverse and deg*keV for longitudinal. The beam envelopes are shown at the bottom, following the same color convention. The location and lengths of quadrupoles are represented by the squares labeled Q. Drifts are represented by a black horizontal line at the lower graph midplane. Finally, the numbers on the lower graph, spanning 1 to 18, sequentially label all elements called in the simulation. Quadrupole gradients are shown in Table 6.

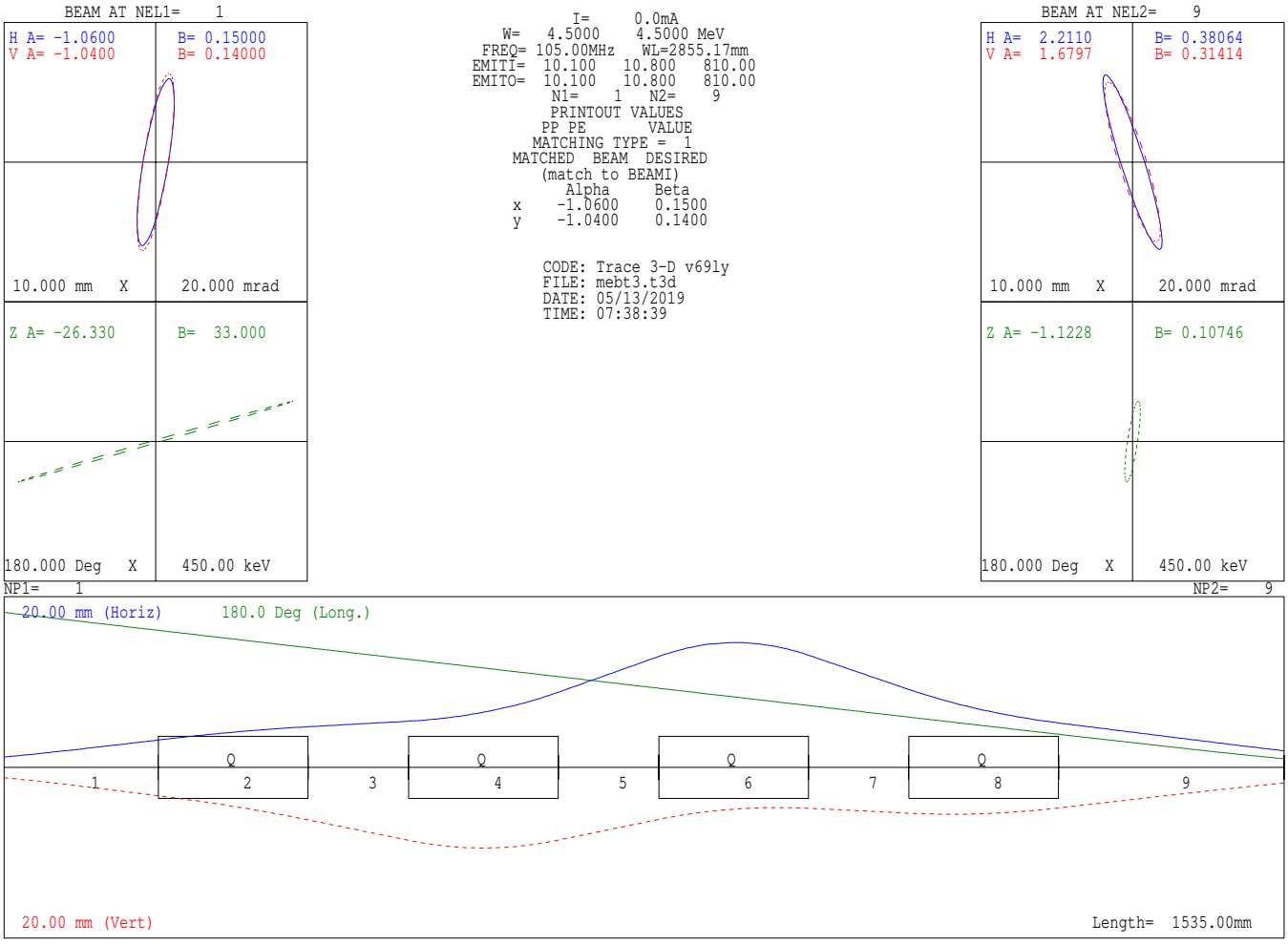

Figure 13: `Trace-3D` envelope simulation of sub-sequence spanning MEBT:Q10 to MEBT:Q13. The horizontal envelope and its parameters are shown in blue, horizontal in red and longitudinal in green. The input beam ellipses containing $4\epsilon_{RMS}$ are shown on the left hand side, with A and B representing the Twiss parameters α and β, while the output distributions are on the right hand side. The input and output beam emittances are visible in the top center, labeled EMITI and EMITO, respectively, and have units of mm*mrad for transverse and deg*keV for longitudinal. The beam envelopes are shown at the bottom, following the same color convention. The location and lengths of quadrupoles are represented by the squares labeled Q. Drifts are represented by a black horizontal line at the lower graph midplane. Finally, the numbers on the lower graph, spanning 1 to 9, sequentially label all elements called in the simulation. Quadrupole gradients are shown in Table 6.

4.2 Trace-3D Element Setpoints

The MEBT quadrupole magnetic field gradients produced by Trace-3D for the MEBT envelopes shown in Section 4.1 are shown in Table 6. Note that Trace-3D does note define quadrupole apertures and as such produces field gradients. On the other hand, TRANSOPTR does define magnet aperture radius and defines the quadrupole strength using the pole tip field.More information on ISAC HE quadrupoles may be found in [19].

Magnet	Aperture [cm]	Gradient [T/m]
MEBT:Q1	2.6	13.9353
MEBT:Q2	2.6	−18.8808
MEBT:Q3	2.6	4.5847
MEBT:Q4	2.6	16.8600
MEBT:Q5	2.6	−18.7872
	$Q:1\longrightarrow 5$	
MEBT:Q6	2.6	−11.5733
MEBT:Q7	2.6	7.4497
MEBT:Q8	2.6	7.4497
MEBT:Q9	2.6	−11.5733
MEBT:Q10	2.6	2.9500
MEBT:Q11	2.6	−8.1400
MEBT:Q12	2.6	8.9700
MEBT:Q13	2.6	−5.6400

Table 6: Trace-3D MEBT quadrupole field gradients for the envelope simulations shown in Figures 11, 12 & 13, corresponding to an A/q = 30, 0.15MeV/u RFQ output beam injected in the MEBT section. The beam is stripped to a charge state of 5 at the foil, between MEBT:Q5 and Q6.

4.3 TRANSOPTR Simulation of the MEBT Beamline

The sequence mebt_db0 in the /acc database was used to generate three separate TRANSOPTR sy.f call stacks, which represent the identical sub-sequences used for the Trace-3D simulations shown in Figures 11, 12 and 13. For the purposes of this simulation, the Rebuncher was omitted from the final sequence, to closely replicate the original simulation. The envelopes were extracted from Trace-3D and overlayed to the TRANSOPTR ones for each of the subsequences, with the results presented in Figure 14.

Regarding the amplitude setting of the bunch rotator for Figure 14, the TRANSOPTR value was found at 4.2MV/m which, considering the central rotator gap of 1.38cm, corresponds to approximately ±30kV applied on the two central tubes of the cavity, to produce a time focus at the stripping foil location. This figure is consistent with the quoted maximum value

of $\pm$35.5kV, noted in reference [20].

In terms of agreement, it is noted that the envelopes qualitatively agree for each of the sub-sequences shown in Figure 14. A quantitative comparison between the model envelopes was performed via `python`. All datasets from `TRANSOPTR` and `Trace-3D` were linearly interpolated, and the difference in percentage computed, shown in Figure 15.

For all sub-sequences and envelopes, both transverse and longitudinal envelope disagreement between models remains bound between $\pm$0.05cm. Such a small maximum error lies within the approximate detection threshold of the beam diagnostic equipment in the MEBT section, for example rotary position monitors (RPMs). In the longitudinal dimensions, given the MEBT design beam energy of 0.15MeV/u (RFQ output energy), a 0.05cm longitudinal envelope discrepancy corresponds to a time interval:

$$K = (\gamma - 1)mc^2$$
$$\gamma = \frac{K}{mc^2} + 1$$

which, for the values used in the present simulation, from Table 5:

$$\gamma = \frac{4.50}{27944} + 1$$
$$\beta = \sqrt{(1 - \frac{1}{\gamma^2})}$$
$$\beta = 0.0179$$

inserting the maximum order of magnitude error value of 0.05cm, this produces a longitudinal bunch length in units of time corresponding to:

$$\Delta t = \frac{z}{\beta c}$$
$$\Delta t \sim 0.09ns$$

which means a timewidth error on the order of one tenth of one nanosecond, which is near the resolution threshold for the time-resolving fast faraday cup in the MEBT section.

For the transverse case, to understand the magnitude of a 0.05cm beam envelope discrepancy, it is useful to consider the rotary position monitors (RPMs) in MEBT, which follow the standard ISAC design. the devices read in the beam current distribution in both x and y, producing a position-dependant current readback, revealing the envelope. The current vs position readings are discretized on a 500 point grid, and the x and y domains spas 1 inch each. This roughly corresponds to approximately 0.002inch/datapoint, or 0.005cm/datapoint, meaning an envelope variation of this magnitude would be difficult to discern on the RPM readback utility.

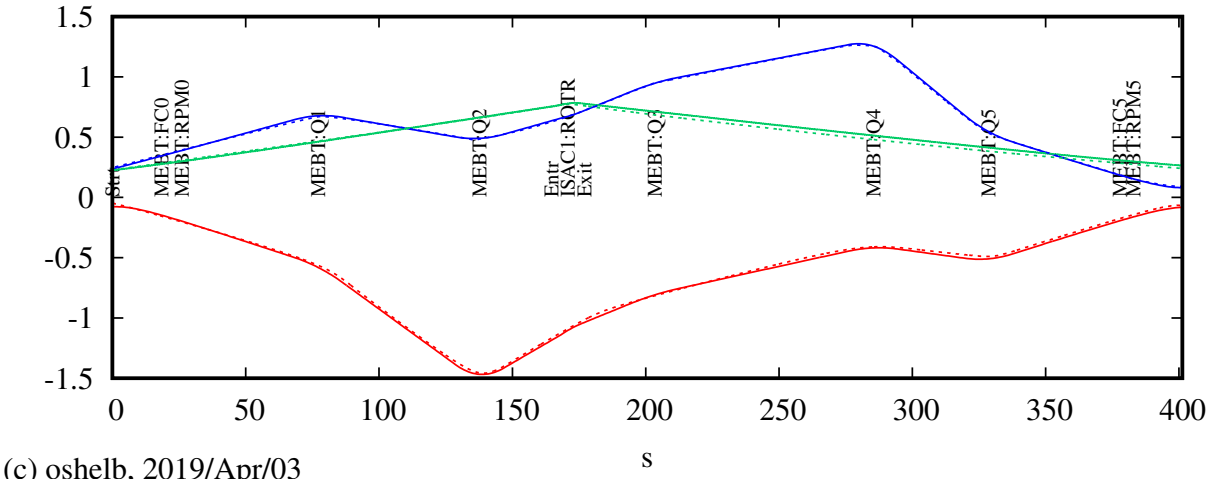

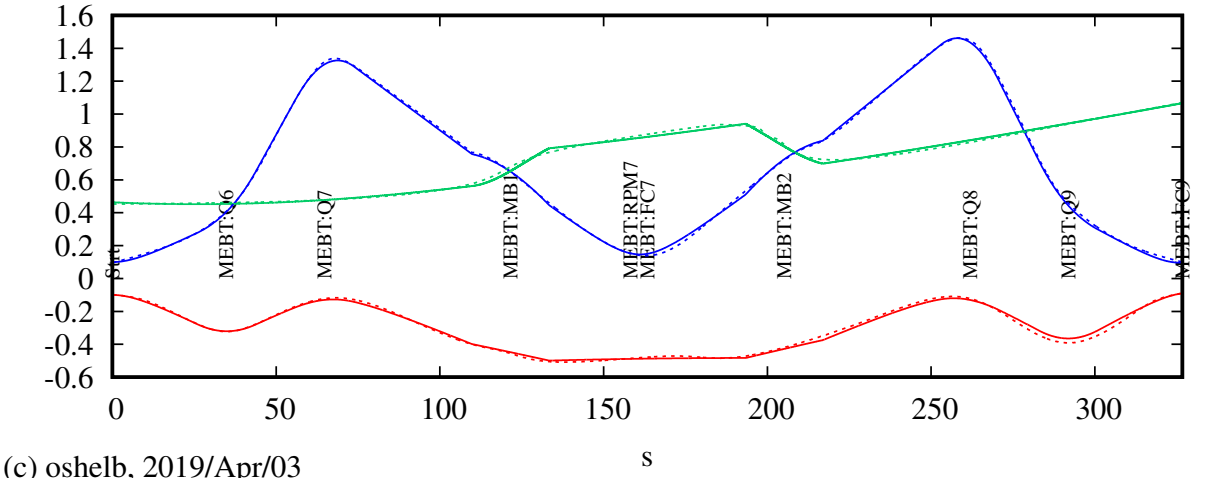

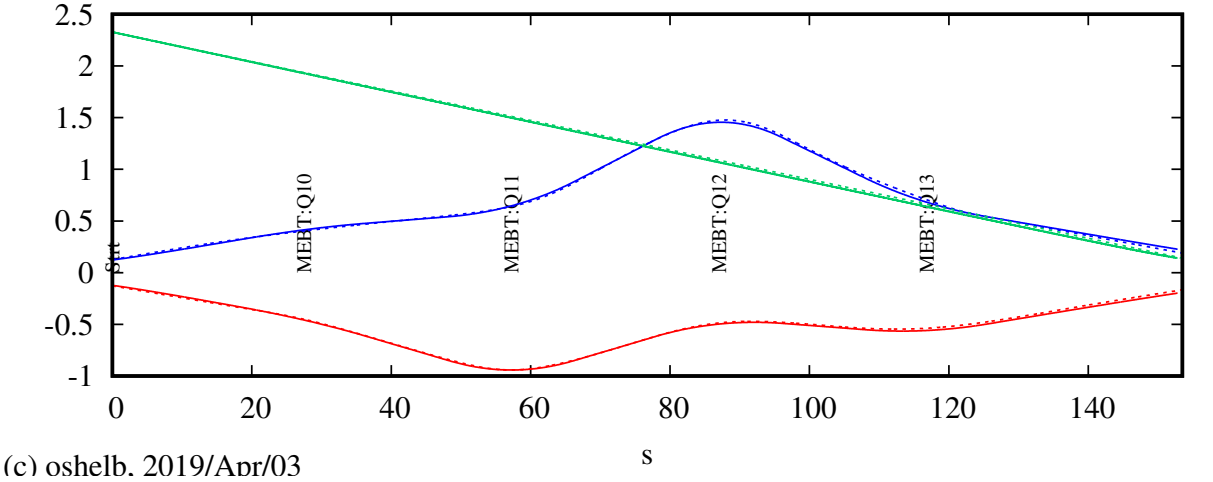

Figure 14: `TRANSOPTR` envelope simulation (solid lines), overlayed with the `Trace-3D` envelope (dashed lines), for the sub-sequences spanning MEBT:Q1 to Q5 (top), MEBT:Q6 to Q9 (middle) and MEBT:Q10 to Q13 (bottom). The horizontal envelopes are shown in blue, vertical in red and longitudinal in green. Element names, as represented in the `TRANSOPTR` sequence `mebt_db0` are shown vertically at the graph midplanes. All x and y-axis dimensions are in cm.

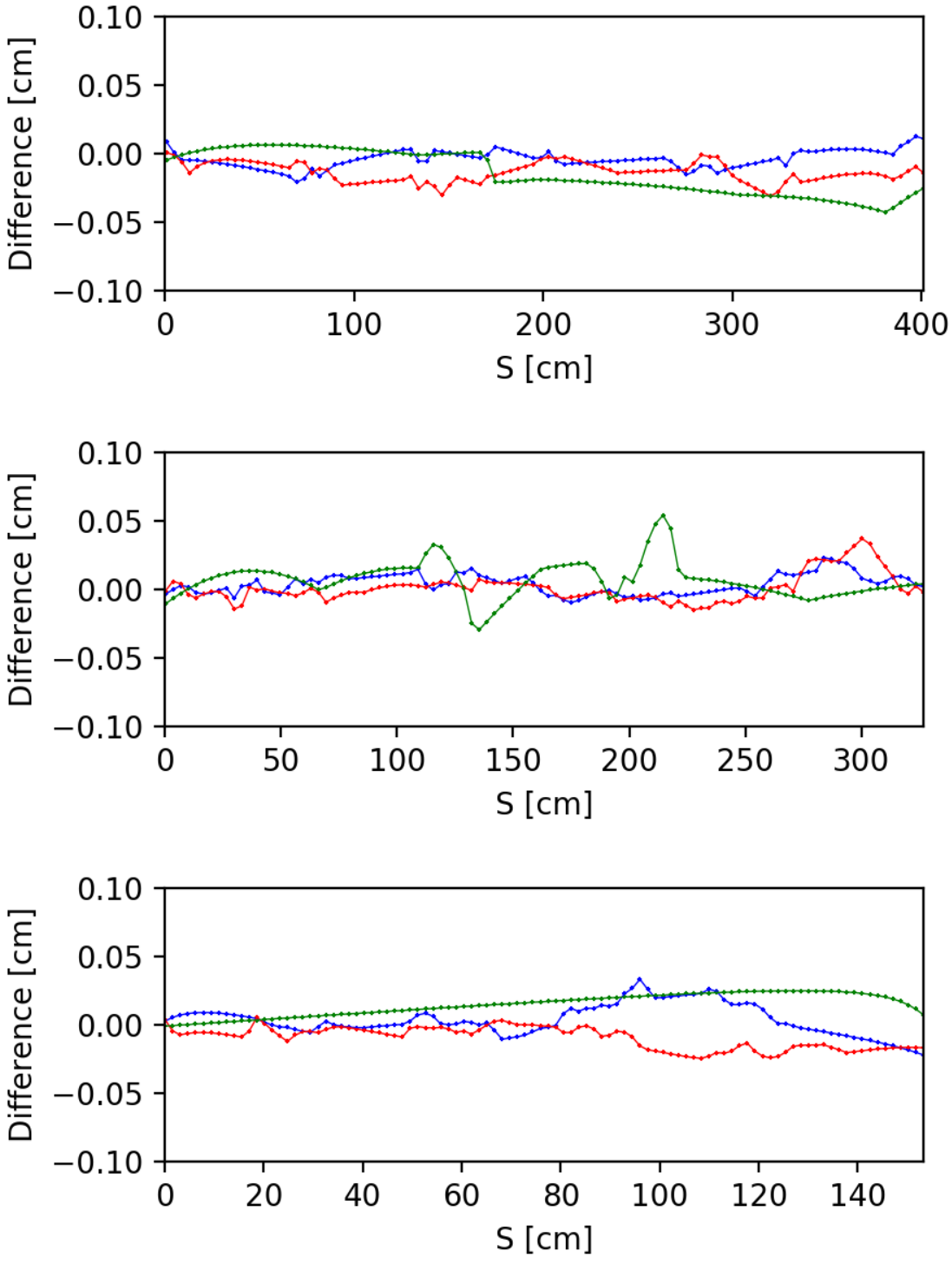

Figure 15: `TRANSOPTR-Trace-3D` envelope residual error in cm, for the sub-sequences spanning MEBT:Q1 to Q5 (top), MEBT:Q6 to Q9 (middle) and MEBT:Q10 to Q13 (bottom). The horizontal envelope differences are shown in blue, vertical in red and longitudinal in green.

5 Conclusion

In this note, a novel implementation of the envelope code TRANSOPTR, via the TRIUMF High-Level Applications framework was demonstrated to produce simulations consistent with the envelope code Trace-3D. The former was, up until 2019, used as the standard tool for envelope analysis and tune computation for the ISAC-MEBT section. Qualitative and quantitative comparison of envelope simulations from both codes demonstrate a strong agreement in terms of both transverse and longitudinal envelope behavior along the MEBT section. As such, it is reasonable to conclude that, in terms of performance and capability, the present TRANSOPTR implementation for the MEBT section is at least equivalent to that offered by Trace-3D, paving the way for the extension of the former as the premier simulation package for ISAC high energy tuning and analysis. In addition, the present implementation is a central requirement for the establishment of an end-to-end model for ISAC-I accelerators.

A possible point of further development for the MEBT simulation would be the implementation of a custom TRANSOPTR subroutine of the MEBT quadrupoles. At present, each quadrupole calls the subroutine MQUAD, which is supplied with an 18.0cm effective length. While this can be considered a first order simulation, a refinement would be to use the measured quadrupole effective length for each device, in addition to the implementation of a realistic fringe field, which would add to the accuracy of the simulation.

As a measure of completeness, it is reiterated that the present investigation does not claim to make a commentary on the performance of either model. Further, it is reiterated that more calibration work is necessary with regards to the TRANSOPTR implementation of the bunching cavities, namely the Bunch Rotator and the MEBT Rebuncher. However, the present work does demonstrate that a high degree of longitudinal envelope agreement may be reached between models, for physically plausible voltages applied on the TRANSOPTR modelled Bunch Rotator, namely $\pm \sim$35kV on the central tubes.

References

[1] Heighway EA and Hutcheon RM. *TRANSOPTR - A SECOND ORDER BEAM TRANSPORT DESIGN CODE WITH OPTIMIZATION AND CONSTRAINTS*. Technical report, Atomic Energy of Canada Limited, 1981.

[2] Baartman R. *TRANSOPTR Changes Since 1984*. Technical Report TRI-BN-16-06, TRIUMF, 06 2016.

[3] Sacherer FJ. *RMS Envelope Equations With Space Charge*. Technical report, CERN, 1970.

[4] RE Laxdal and M Marchetto. *The ISAC post-accelerator*. *Hyperfine Interactions*, 225(1-3):79–97, 2014.

[5] R Tiede, U Ratzinger, H Podlech, and C Zhang. *KONUS Beam Dynamics Designs Using H-Mode Cavities*. In *Proceedings Hadron Beam 2008*, pages 223–30, 2008.

[6] Koscelniak S. *Design History of the ISAC RFQ*. Technical Report TRI-DN-95-04, TRIUMF, 02 1995.

[7] Barquest C. *Web-Based Control Room Applications at TRIUMF*. In *Proceedings of the 9th International Particle Accelerator Conference*, pages 4832–35, 2018.

[8] Stinson GM. *A design for short quadrupoles for the ISAC MEBT beam line*. Technical Report TRI-DNA-97-01, TRIUMF, 1997.

[9] Laxdal RE. *Charge Distribution and Beam Loss after MEBT Foil*. Technical Report TRI-DNA-99-27, TRIUMF, 1999.

[10] Baartman R. *Fast Envelope Tracking for Space Charge Dominated Injectors*. In *Proceedings of LINAC 2016 Conference*, pages 1017–21, 2016.

[11] Bricault P, Poirier R, Ries T, Roper R, and Standford S. *Tank1 of the ISAC-DTL Linac*. In *Proceedings of the 1999 Particle Accelerator Conference, New York, NY*, pages 3540–42, 1999.

[12] Bylinsky YV, Kvasha AI, Menshov AA, Ostroumov PN, and Paramonov VV. *High Power Test of the ISAC Triple Gap Buncher Operating in CW Mode*. In *Proceedings of the 1999 Particle Accelerator Conference, New York, NY*, pages 893–985, 1999.

[13] Bricault P, Duto G, Laxdal R, and et al. Mitra A. *Status Report on the Construction of the ISAC Drift Tube Linac*. In *Proceedings of the XX International Linac Conference, Monterrey, CA*, pages 208–10, 2000.

[14] Mitra AK and Poirier RL. *High Power Test of the 35 MHz Spiral Re-Buncher Cavity for the TRIUMF ISAC Facility*. In *Proceedings of EPAC 2000, Vienna, Austria*, pages 1978–80, 2000.

[15] Vasyuchenko A, Feschenko A, Kvasha A, Menshov A, and Paramonov V et al. *Development, Fabrication and Test of Triple Gap Split-Ring Bunchers for the TRIUMF ISAC Facility*. In *Proceedings of the 2001 Particle Accelerator Conference, Chicago, IL*, pages 978–80, 2001.

[16] Mitchell M, Muftakhidinov B, Winchen T, et al. *Engauge digitizer software*. *Webpage: http://markummitchell. github. io/engauge-digitizer. Accessed*, 11, 2017.

[17] Vector Fields. *Opera-2d user guide*. *Vector Fields Limited, England*, 1999.

[18] KR Crandall. *TRACE3d documentation, Los Alamos Accelerator Code Group*. Technical report, LAUR-90-4146, 1990.

[19] R. Baartman. *B-I Curve fits for TRIUMF Quads*. Technical Report TRI-DN-07-04, TRIUMF, 2007.

[20] AK Mitra, PJ Bricault, IV Bylinskii, K Fong, G Dutto, RE Laxdal, RL Poirier, et al. *RF Test and Commissioning of the Radio Frequency Structures of the TRIUMF ISAC I facility*. In *Proceedings of LINAC*, page 106, 2002.